Thermal and Mass Transport Enhancements in Casson Ternary Hybrid Nanofluid Flow through an Exponentially Stretching Cylinder: Accounting for Darcy-Forchheimer and Arrhenius Effects

Jintu Mani Nath[1], Ali J. Chamkha[2], Ashish Paul[3,*], Tusar Kanti Das[4]

[1]Department of Mathematics, Mangaldai College, Mangaldai-784125, India

[2]Faculty of Engineering, Kuwait College of Science and Technology, Doha District-35004, Kuwait

[1,3,4]Department of Mathematics, Cotton University, Guwahati-781001, India

[4]Department of Mathematics, Dudhnoi College, Dudhnoi-783124, Assam, India

[1]Email: jmnath1995@gmail.com

[2]Email: a.chamkha@kcst.edu.kw

[3,*]Email: ashish.paul@cottonuniversity.ac.in

[3,*]Contact Number: +917002958863

[4]Email: tusarkantidas1995@gmail.com

[*]Corresponding Author

ABSTRACT:

The primary goal of this study is to investigate the shear-thinning ternary hybrid magnetohydrodynamics nanofluid flow through an exponentially stretched cylinder incorporating Arrhenius energy and varying thermal conductivity. Darcy-forchheimer impact and a magnetic field are also employed in this flow model. The Casson ternary hybrid nanofluid mechanism is utilized in conjunction with Molybdenum disulfide, Silver, and Copper nanoparticles. The assortment of partial differential equations (PDEs) in the mathematical framework is simplified to ordinary differential equations (ODEs) by implementing the similarity transformation. MATLAB computing approach Bvp4c is used to achieve the numerical solutions for regulating ODEs and portray the graphs for numerous emerging variables. The core findings indicate that the non-Newtonian ternary hybrid nanofluid highlights a more noticeable thermal and mass transport enrichment than the hybrid nanofluid. The thermal transmission rate for polymer-based trihybrid nanofluid is almost 3% superior in contrast to hybrid nanofluid. Also, the absolute shear rate for ternary hybrid nanofluid is nearly 5.02% better than the hybrid nanofluid. Additionally, the research significantly advances the forecasting of the significance of shear-thinning ternary hybrid nanofluid in the thermal transport processes. The findings reflect strong consistency with earlier released studies.

KEYWORDS: Casson fluid, Ternary hybrid nanofluid, Arrhenius energy, Darcy–Forchheimer, Heat transport, Variable thermal conductivity

1. INTRODUCTION:

The broad spectrum of nanofluid applications has resulted in the development of the scientific study of nanofluids in recent years. Various nanoparticles must be incorporated into the base fluids to optimize the heat conductivity of typical fluids such as ethylene glycol, water, kerosene, and engine oils. Choi was the initial one to propose the notion of a nanofluid, which is essentially an entirely novel type of fluid involving the dispersion of metal fragments into ordinary fluids to boost thermal conductivity. Enhanced thermal conductivity and stronger heat transport are prominent benefits of integrating nanoparticles. A substantial number of studies have been identified that are focused on improving the carrying fluid's thermal conductivity with the inclusion of several kinds of

nanoparticles. Kakaç and Pramuanjaroenkij [1] addressed the convective thermal transport enrichment with nanofluids. Also, Kumar and Sarviya [2] reviewed the current progress in the preparation of nanofluids for thermal transfer escalation in thermal exchangers. Shrestha et al. [3] investigated the liquid volume and squeeze force impacts on nasal irrigation employing volume of fluid modeling. Moreover, Arulmozhi et al. [4] explored the thermal and mass transport exploration of radiative and chemical reactive impacts on MHD nanofluid via an infinite moving vertical plate. Also, Reddy and Mangamma [5] investigated the importance of radiation and chemical reactions on MHD thermal transport nanofluid flow incorporating a non-uniform thermal source.

Hybrid nanofluids were developed to ameliorate stability, alleviate pressure drop, enhance thermal conductivity, and, most significantly, optimize the synergistic impacts of nanoparticles. The hybrid nanofluid has a substantially larger heat conductivity in contrast to nanofluids. Spreading a pair of numerous types of Nanoparticles into the fundamental fluid is the mechanism that produces hybrid nanofluids. In recent days, a multitude of explorers have examined the flow of distinct hybrid nanofluids past distinct interfaces. Ahmed et al. [6] scrutinized the thermal and mass transport attributes of copper–aluminum oxide hybrid nanoparticles in porous media. Furthermore, Kavya et al. [7] delved into Magneto-hybrid nanoparticles along a stretching/shrinking cylinder suspended in MoS_2 and Cu nanoparticles. Also, Vijatha and Reddy [8] addressed the entropy optimization of magneto-hybrid nanofluid movement along the Cattaneo-Christov thermo flux model. Moreover, Paul et al. [9] computationally analyzed MHD Casson hybrid nanofluid flow via an exponentially stretched cylinder. Subsequently, Paul et al. [10, 11] investigated thermally stratified hybrid nanofluid flow via an extending cylinder, considering multiple influences. Recently, Chu et al. [12] performed a comparative investigation of unsteady magnetohydrodynamics hybrid nanofluid movement between two infinite parallel plates. Shamshuddin et al. [13] computationally conducted an analysis for silica-molybdenum disulfide/water-driven hybrid nanofluid via an exponential stretching sheet integrating a spectral quasi-linearization method. Also, Shamshuddin et al. [14] addressed the bioconvective treatment for the Casson hybrid nanofluid movement via an exponentially stretching sheet incorporating Ohmic heating and combined convection influence. Also, Lone et al. [15] analyzed the MHD-driven bioconvective movement of hybrid Casson nanofluid across a permeable exponential stretching sheet. After that, Tamanna et al. [16] numerically investigated the thermal transportation elevation on Tangent Hyperbolic hybrid nanofluid Fluid movement across a Stretching Sheet incorporating an Inclined Magnetic Field. Also, Yasmin et al. [17] investigated the computational outcome for swirling hybrid nanofluid movement incorporating silver/gold nano-crystals on a stretching cylinder with thermal source/sink. Furthermore, Shamshuddin et al. [18] examined the homotopic simulation of MHD bioconvective movement of water-driven hybrid nanofluid via a thermally convective exponential stretching surface.
In a piece of recent research, three numerous kinds of nanoparticles are embedded in one sort of fluid for creating "ternary hybrid nanofluids". The thermal evaluation of a newly patented notion for ternary hybrid nanofluids with differently shaped nanoparticles demonstrates an intriguing thermal transfer rate throughout multiple sectors. The investigation conducted by Manjunatha et al. [19] inspected the implications of the magnetic impacts on the movement of ternary hybrid nanofluid through a stretched sheet. Also, Alharbi et al.'s research [20] centered on the quantitative assessment of a hybrid Darcy ternary nanofluid flow over a prolonged cylinder exhibiting induction ramifications. Furthermore, the simulation of the transportation of heat and mass for aiding and resisting radiative flows transporting ternary hybrid nanofluid throughout an exponentially stretched surface was addressed by Nagaraja et al. [21]. Mumtaz et al. [22] probed the thermal dissemination abilities of a ternary hybrid nanofluid flowing through a curved extended sheet.

The idea of "activation energy" symbolizes the minimum amount of energy that molecules or atoms need to gather to trigger a chemical process. It was first proposed by Svante Arrhenius in 1889. Chemical mechanisms comprising the transfer of mass and activation energy are necessary in oil storage tanks, water-and-oil emulsions, processing of food, as well as other disciplines. The Research on the

convective thermal transport performance and Arrhenius activation energy in radiative hybrid nanofluid flow was performed by Jayaprakash et al. [23]. In their exploration, Rekha et al. [24] explored the bearing of activation energy on the water-based hybrid nanofluid flow through three distinct surfaces. Mishra et al.'s study [25] addressed the entropy enlargement of a cilia-regulated MHD ternary hybrid Jeffrey nanofluid featuring Arrhenius activation energy and an imposed magnetic field. Puneeth et al. [26] also determined the stratified bio-convective jet flow of Williamson nanofluid in a porous region considering Arrhenius energy.

In the course of that period, an abundance of researchers has been paying particular attention to the varying thermal conductivity impact. Plenty of studies have been performed on heat and mass transfer, but there remains much to learn about changing thermal conductivity through a stretched cylinder using an efficient and trustworthy computational approach. Zubair et al. [27] performed a numerical exploration of the non-Newtonian hybrid nanofluid featuring variable thermal conductivity. Eid and Nafe's exploration [28] focused on the influence of generated heat and changes in thermal conductivity on magneto-hybrid nanofluid flow. The consequences of combined convection and varying thermal conductivity on hybrid nanofluid circulation throughout an extended sheet under slip constraints were explored by Manigandan and Satya Narayana [29]. The implications of changing heat conductivity on the flow of a trihybrid nanofluid via a stretching surface were considered by Jan et al. [30] in their investigation.

A lot of scholars have become fascinated by the Darcy-Forchheimer phenomena during this period. The utilization of ultra-filtering procedures in drugs, leakage of water at extreme levels in natural lakes and reservoirs, waste from commercial shipping, and the penetration of substances with large permeability over chemicals beneath engineering structures are a few examples of practical consequences of Darcy-Forchheimer's impact. In a case study of an expanding sheet, Gautam et al. [31] inspected the impacts of the activating energy and binary chemical reaction on the nanofluid flow in a Darcy-Forchheimer porous medium. After that, the investigation carried out by Rahman et al. [32] addressed the assessment of invincibility in viscous nanomaterial flow utilizing Darcy-Forchheimer with the energy of activation. Haq et al. [33] computationally simulated the MHD flow of hybrid nanofluid incorporating Darcy–Forchheimer impact across an extending domain. Alqahtani et al.'s [34] investigation focused on the thermal and mass transmission throughout an exponentially stretched stretching sheet employing MHD Darcy Forchheimer Casson hybrid nanofluid movement. Recently, Ramasekhar and Reddy [35] explored the entropy generation on the Darcy-Forchheimer movement of water-driven Cu/Al_2O_3 hybrid nanofluid via a rotating disk.

Non-Newtonian fluid can be classified as a fluid, in which the viscosity is contingent on its shear-thinning/thickening attributes. In light of viscosity dependability assets numerous fluid frameworks have been designed, like Casson fluid, Maxwell fluid, etc. Plenty of engineering disciplines, notably crude oil, the printing process, preserving food, and fiber optics industries, exploit non-Newtonian fluids. The Casson fluid model acquired its name in recognition of its creator, Casson. A lot of scholars have an appetite for Casson nanotechnology in contemporary times. There is a noteworthy influence on blood flow from the Casson nanofluid. Zeeshan et al. [36] addressed the Casson tri-hybrid nanofluid involving the consequences of radiation. Furthermore, Turabi et al. [37] looked into the convective transportation processes in tri Casson hybrid nanofluid stream in an upward tube with heat-generating repercussions. They asserted that temperature climbs with rising Eckert number. Ali et al. [38] explored the thermal transportation of turbulent slip movement of ternary hybrid Casson fluid across irregular stretching discs.

The prevailing literature mentioned above indicates that there has been no prior study into a polymer-

driven non-Newtonian ternary hybrid nanofluid composed of *Ag*, MoS_2, and *Cu* nanoparticles flowing over an exponentially stretched cylinder considering the effects of Activation energy, Darcy–Forchhei mer, and chemical reaction. The present research incorporates another level of quality to the analysis b y integrating variable thermal conductivity. This is a possible research gap that requires discussion. T he governing equations are modeled under various assumptions and then computationally solved throu gh the MATLAB bvp4c method. This investigation reflects an enormous advancement in the domain o f fluid dynamics and heat transmission due to its extensive uniqueness.
The novel aspects of this research are to feature the following research questions:

i) What consequences have been imparted by the nanoparticles *Ag*, MoS_2, and *Cu* over the flow, thermal, and solutal characteristics of the proposed model?
ii) How does the thermal and mass transportation n rate fluctuate in the context of hybrid and ternary hybrid nanofluid across the exponential stretching cylinder?
iii) What inside can be procured due to the influence of Activation energy on the outline of thermal trajectory?
iv) How does the nonlinear Darcy factor have a significant impact on chemically reactive ternary Casson hybrid nanofluid flow?
v) How does the variation in thermal conductivity cause an impact on the proposed flow geometry?

The core purpose of the current investigation is to investigate the influences of the governing factors, namely the Activation energy term, Schmidt number, Darcy-Forchheimer factor, Porosity Parameter, Variable conductivity term, Chemical reaction factor, Temperature ratio term, Casson term, and the Magnetic term on the velocity, thermal and solutal trajectory as well as the skin friction coefficient, the Nusselt number, and the Sherwood number. The current study also comprehensively compared two different fluid flow circumstances, including the flow of hybrid nanofluid and ternary hybrid nanofluid through pictorial and tabular forms. This study highlights the intricate interactions between the above-mentioned impacts in the shear-thinning ternary hybrid nanofluid flow. As per the authors' concern, this kind of discovery has not been explored in this geometry featuring the aforementioned effects, which provides the novelty to the proposed model. With so many practical consequences and an entirely novel trajectory for the field, this work attracts academics and industry specialists eager to apply these innovative findings to promote innovation and efficiency in an assortment of manufacturing processes. Numerous fields, including solar energy systems, healthcare equipment, nuclear power plants, and the aerospace industry, can benefit from the wide range of potential uses of this theoretical framework. This study is expected to make a distinct contribution to the forecasting of shear-thinning ternary hybrid nanofluid's significance in thermal transmission processes.

2. MATHEMATICAL FORMULATION:

This work addresses two-dimensional polymer-based non-Newtonian ternary hybrid nanofluid flow over an exponentially stretched cylinder in the context of the chemical reaction, based on the boundary layer strategy and steady laminar flow condition. The aforementioned flow problem is analyzed in terms of the cylindrical polar (z, r) coordinate system, where the radial direction is indicated by r and the axial direction by z. As illustrated in Figure 1, this flow is described by induced Lorentz force (B_0) in the convective flow region, and the exponentially stretching surface is considered to move through the velocity $w_w = 2ac\exp\left(\frac{z}{a}\right)$, where c and a indicate the rate of stretching and cylinder's base radius respectively. The wall temperature (T_w) and wall concentration (C_w) are considered as

$T_w = T_\infty + A^* \exp\left(\frac{z}{a}\right)$ and $C_w = C_\infty + B^* \exp\left(\frac{z}{a}\right)$, where A^*, B^*, T_∞ and C_∞ indicates the positive constants, temperature and concentration at the ambient respectively. Also, the effects of Activation energy, Darcy–Forchheimer media, and varying thermal conductivity are taken in this flow model. The variable thermal conductivity is considered to be differ with temperature as $k_{hnf}(T) = k_{hnf}\left(1+ \in \theta(\eta)\right)$, where $\epsilon$is demonstrated as a variable thermal conductivity factor.

Applying the aforementioned supposition, the constitutive regulating equations acquire the following form:(Ref. [10], [39])

Continuity Equation

$$\frac{\partial u}{\partial r} + \frac{u}{r} + \frac{\partial w}{\partial z} = 0 \tag{1}$$

Momentum Equation

$$u\frac{\partial w}{\partial r} + w\frac{\partial w}{\partial z} = \frac{\mu_{thnf}}{\rho_{thnf}}\left(1+\frac{1}{B}\right)\left[\frac{\partial^2 w}{\partial r^2} + \frac{1}{r}\frac{\partial w}{\partial r}\right] - \frac{\sigma_{thnf}}{\rho_{thnf}}B_0^2 w - \frac{\mu_{thnf}}{\rho_{thnf}}\left(1+\frac{1}{B}\right)\frac{1}{k_p}w - \frac{C_b}{\sqrt{k_p}}w^2 \tag{2}$$

Energy Equation

$$u\frac{\partial T}{\partial r} + w\frac{\partial T}{\partial z} = \frac{1}{r}\frac{\partial}{\partial r}\left(k_{thnf}(T)\, r\frac{\partial T}{\partial r}\right) \tag{3}$$

Concentration Equation

$$u\frac{\partial C}{\partial r} + w\frac{\partial C}{\partial z} = D\left(\frac{1}{r}\frac{\partial C}{\partial r} + \frac{\partial^2 C}{\partial r^2}\right) - k_r^2 (C - C_\infty)\left(\frac{T}{T_\infty}\right)^N \exp\left(\frac{E_a}{K_1 T}\right) \tag{4}$$

Constraints within boundaries are:

$$w(a,z) = w_w, u(a,z) = 0, T(a,z) = T_w(z), C(a,z) = C_w(z) \text{ whenever } r = a$$

$$w(r,z) \to 0, T(r,z) \to 0, C(r,z) \to 0 \text{ whenever } r \to \infty \tag{5}$$

Where, (u, w) symbolizes the velocity components run along (r, z) direction. The activation Arrhenius parameter $k_r^2\left(\frac{T}{T_\infty}\right)^N \exp\left(\frac{Ea}{k_1 T}\right)$ is indicated in the concentration equation incorporating the Boltzmann constant k_1, where $-1 < N < 1$.

The variables we utilized for the Similarity Transformation in the present scenario are as follows (Ref. [9]):

$$\eta = \left(\frac{r}{a}\right)^2, w = w_w f^{'}(\eta), u = -\frac{1}{2} w_w \frac{f(\eta)}{\sqrt{\eta}},$$

$$\theta = \frac{T - T_\infty}{T_W - T_\infty}, \phi = \frac{C - C_\infty}{C_w - C_\infty}$$

The converted coupled ODEs can be displayed as follows:

$$f^{'2} - ff^{"} = \frac{1}{\mathrm{Re}} \frac{\mu_{thnf}}{\mu_f} \frac{\rho_f}{\rho_{thnf}} \left(1 + \frac{1}{B}\right) \left[(\eta f^{'''} + f^{"})\right] - \frac{\sigma_{thnf}}{\sigma_f} \frac{\rho_f}{\rho_{thnf}} M.f^{'} - \frac{\mu_{thnf}}{\mu_f} \frac{\rho_f}{\rho_{thnf}} \frac{P}{\mathrm{Re}} \left(1 + \frac{1}{B}\right) f^{'} - Fr.f^{'2} \tag{6}$$

$$\mathrm{Pr.Re}\left(f^{'}\theta - f\theta^{'}\right) = \frac{\left(\rho C_p\right)_f}{\left(\rho C_p\right)_{thnf}} \left(\frac{k_{thnf}}{k_f}\right) \left(\in \eta\theta^{'2} + (1 + \in \theta)\left(\eta\theta^{"} + \theta^{'}\right)\right) \tag{7}$$

$$\left(f^{'}\phi - f\phi^{'}\right) = \frac{1}{\mathrm{Re}} \frac{1}{Sc} \left(\eta\phi^{"} + \phi^{'}\right) - Cr\left(1 + \gamma\theta\right)^N \exp\left(-\frac{E}{1 + \gamma\theta}\right)\phi \tag{8}$$

The converted boundary limitations are

$$f(0) = 0,\ f^{'}(0) = 1, \theta(0) = 1, \phi(0) = 1 \tag{9}$$

$$f^{'}(\infty) = 0, \theta(\infty) = 0, \phi(\infty) = 0 \tag{10}$$

Here,

$$\mathrm{Pr} = \frac{\nu_f}{\alpha_f}, \mathrm{Re} = \frac{a w_w}{4\nu_f}, M = \frac{\sigma_f B_0^2 a}{\rho_f w_w}, Cr = \frac{K_r^2 a}{w_w}, E = \frac{E_a}{K_1 T_\infty}, \gamma = \frac{T_w - T_\infty}{T_\infty}$$

$$Sc = \frac{\nu_f}{D_f}, Fr = \frac{c_b a}{\sqrt{k_p}}, P = \frac{a^2}{4k_p}$$

The physical factors of scientific interest in this flow model are the coefficient of drag force i.e. skin friction coefficient, Nusselt number, and Sherwood number, which physically indicates the tangential stress, the rate of thermal transport, and the rate of mass transmission at the surface respectively.

Skin Friction Co-efficient:

$$\tau_w = \mu_{hnf} \left(1 + \frac{1}{B}\right) \left(\frac{\partial w}{\partial r}\right)$$

Nusselt Number:

$$Nu_z = \frac{a\exp\left(\frac{z}{a}\right)q_w}{k_f\left(T_w - T_\infty\right)}, \text{ where } q_w = -k_{tnf(T)}\left(\frac{\partial T}{\partial r}\right)_{r=a}$$

Sherwood Number:

$$Sh_z = \frac{a\exp\left(\frac{z}{a}\right)q_m}{D\left(C_w - C_\infty\right)}, \text{ where } q_m = D\left(\frac{\partial C}{\partial r}\right)_{r=a}$$

The amended Skin friction, Nusselt Number, and Sherwood Number can be expressed as follows by using the similarity conversion variables:

$$C_f \,\mathrm{Re}_z^{\frac{1}{z}} = \frac{\mu_{thnf}}{\mu_f}\left(1+\frac{1}{B}\right)\left[f''(1)\right]$$

$$Nu_z \,\mathrm{Re}_z^{-\frac{1}{z}} = -\left(\frac{K_{thnf}}{K_f}\left(1+\in\theta(1)\right)\right)\theta'(1)$$

$$Sh_z \,\mathrm{Re}_z^{-\frac{1}{z}} = -\phi'(1)$$

Thermal Characteristics for the ternary Hybrid nanofluid (Ref. [40], [41]):

***Viscosity*:**

$$\frac{\mu_{thnf}}{\mu_f} = \frac{1}{\left(1-\phi_{Ag}\right)^{2.5}\left(1-\phi_{MoS_2}\right)^{2.5}\left(1-\phi_{Cu}\right)^{2.5}}$$

***Specific Heat capacity*:**

$$\frac{\left(\rho C_p\right)_{thnf}}{\left(\rho C_p\right)_f} = \phi_{MoS_2}\frac{\left(\rho C_p\right)_{MoS_2}}{\left(\rho C_p\right)_f} + \left(1-\phi_{MoS_2}\right)\left[\left(1-\phi_{Ag}\right)\left\{\left(1-\phi_{Cu}\right)+\phi_{Cu}\frac{\left(\rho C_p\right)_{Cu}}{\left(\rho C_p\right)_f}\right\}+\phi_{Ag}\frac{\left(\rho C_p\right)_{Ag}}{\left(\rho C_p\right)_f}\right]$$

D*ensity*:

$$\frac{\rho_{thnf}}{\rho_f} = \left(1-\phi_{Ag}\right)\left[\left(1-\phi_{Ag}\right)\left\{\left(1-\phi_{Cu}\right)+\phi_{Cu}\frac{\rho_{Cu}}{\rho_f}\right\}+\phi_{Ag}\frac{\rho_{Ag}}{\rho_f}\right]+\phi_{MoS_2}\frac{\rho_{MoS_2}}{\rho_f}$$

***Thermal conduction*:**

$$\frac{k_{thnf}}{k_{hnf}}=\left(\frac{k_{Cu}+2k_{hnf}-2\phi_{Cu}\left(k_{hnf}-k_{Cu}\right)}{k_{Cu}+2k_{hnf}+\phi_{Cu}\left(k_{hnf}-k_{Cu}\right)}\right),\frac{k_{hnf}}{k_{nf}}=\left(\frac{k_{MoS_2}+2k_f-2\phi_{MoS_2}\left(k_f-k_{MoS_2}\right)}{k_{MoS_2}+2k_f+\phi_{MoS_2}\left(k_f-k_{MoS_2}\right)}\right),$$

$$\frac{k_{nf}}{k_f}=\left(\frac{k_{Ag}+2k_{nf}-2\phi_{Ag}\left(k_{nf}-k_{Ag}\right)}{k_{Ag}+2k_{nf}+\phi_{Ag}\left(k_{nf}-k_{Ag}\right)}\right)$$

***Electric conductivity*:**

$$\frac{\sigma_{thnf}}{\sigma_{hnf}}=\left(\frac{\sigma_{Cu}+2\sigma_{hnf}-2\phi_{Cu}\left(\sigma_{hnf}-\sigma_{Cu}\right)}{\sigma_{Cu}+2\sigma_{hnf}+\phi_{Cu}\left(\sigma_{hnf}-\sigma_{Cu}\right)}\right),\frac{\sigma_{hnf}}{\sigma_{nf}}=\left(\frac{\sigma_{MoS_2}+2\sigma_{nf}-2\phi_{MoS_2}\left(\sigma_{nf}-\sigma_{MoS_2}\right)}{\sigma_{MoS_2}+2\sigma_{nf}+\phi_{MoS_2}\left(\sigma_{nf}-\sigma_{MoS_2}\right)}\right),$$

$$\frac{\sigma_{nf}}{\sigma_f}=\left(\frac{\sigma_{Ag}+2\sigma_f-2\phi_{Ag}\left(\sigma_f-\sigma_{Ag}\right)}{\sigma_{Ag}+2\sigma_f+\phi_{Ag}\left(\sigma_f-\sigma_{Ag}\right)}\right)$$

3. RESULT AND DISCUSSION:

The pictorial representation of the differential equations system is assessed by a computational MATLAB approach called the "BVP4c methodology". Some of the observations that have been attained are as follows:

3.1 Velocity profile $f'(\eta)$

In Figure 2a-d, the pictorial visualization of velocity $f'(\eta)$ curve against the variation of the magnetic factor M, Darcy Forchhemier factor Fr, Porosity term P, and Casson term B respectively. Figure 2a,b indicates that the fluid velocity distribution minimizes the impact of magnetic factor M and Darcy Forchhemier factor Fr. Physically, Escalating the magnetic factor elicits Lorentz forces, impeding fluid motion and diminishing its velocity distribution. Magnetic fields interact with charged particles, altering their trajectories, restricting movement, and decreasing overall fluid velocity. Also, as the Darcy Forchhemier number escalates, the surface permeability minimizes as well, causing the momentum boundary layer to contract (Paul and Das [39]). Thus, such a circumstance has been reported. Figure 2c further demonstrates how the fluid velocity is influenced by the porosity parameter, P. It's discovered that the fluid's flow declines as P becomes better. Physically, Porosity factor P and porous space diameter k_p is inversely correlated. The porous space diameter goes down as a result of climbing P, creating an obstruction in the flow's path. Due to this impediment, the velocity of the fluid has been dropped in Figure 2c. The consequences of the Casson factor on the velocity curve are portrayed in Figure 2d. While B elevates, the thickness of the boundary layer, and the yield stress is boosted, which improves the fluid viscosity. Hence, the fluid velocity is diminished.

3.2 Thermal profile $\theta(\eta)$

Figure 3a-e exemplifies the reflection of $\theta(\eta)$ curve against the variation of the variable conductivity term ϵ, magnetic term M, Darcy Forchhemier factor Fr, Porosity term P,and Casson term B respectively. Figure 3a demonstrates that the energy $\theta(\eta)$ escalates with the non-negative variation of variable conductivity factor ϵ due to the boost in the heat boundary layer thickness. Also, Figure 3b illustrates the improvement of the thermal profile for boosting the magnetic factor M. Physically, friction is developed due to the Lorentz force, which produces thermal energy. As a consequence, the energy curve is enlarged. On the other hand, the impact of the Darcy–Forchheimer factor Fr is developed, which results in the escalation in the energy curve displayed in Figure 3c. Physically, the fluid flow shifts from a laminar to a turbulent phase while the Darcy-Forchheimer factor elevates(Paul

and Das [39]) . This alteration in flow generates an uptick in frictional losses. This frictional resistive force contributes to the elevation of the thermal curve. Figure 3d exhibits the impacts of the porosity term, P, on the fluid velocity. There is a converse correlation between the porosity parameter P and the porous space diameter k_p. As a consequence, when P enhances, the diameter of the porous space is decreased, which provides a stumbling block in the path of the flow. Due to this obstruction, the heat profile also goes upward. Also, a remarkable elevation in the thermal curve for the Casson term $B$is seen in Figure 3e.

3.3 Concentration Profile $\phi(\eta)$

Figure 4a–f reports the demonstration of concentration $\phi(\eta)$ profile versus the variation of the activation energy term E, chemical reaction factor Cr, Magnetic factor M, Darcy–Forchheimer factor Fr, Schmidt number S, and Casson term B respectively. On the concentration trajectory, Figure 4a exhibits the activation energy's optimizing pattern. The amended Arrhenius function decreases as E escalates. This, in turn, fosters the generative chemical procedure; as a consequence, the concentration of nanoparticles elevates. Also, figure 4b highlights that while the chemical reaction component escalates, the concentration trend steadily diminishes. The reduced concentration field is caused by the fact that whenever the chemical reaction term goes up, the quantity of solute molecules that comprise the reaction simultaneously elevates, leading to a decline in the concentration field. In Figure 4c, the correlation between magnetic term M with the concentration profile portrayed. It has been reported that enhancing the magnetic factor elevates the mass transfer profile. Physically, escalating the magnetic factor enhances concentration profiles via intensified fluid mixing from Lorentz forces. This fosters solute dispersion, facilitating transmission and amplifying concentration gradients within the system. Furthermore, while the Darcy–Forchheimer factor Fr is enhanced, which results in an increment in the concentration profile depicted in Figure 4d. Physically, the flow transitions from a state of laminar to a turbulent mode while the Darcy-Forchheimer factor spikes. The frictional losses are enhanced as a result of the variation in the flow. This force of resistance plays a part in pushing the concentration curve upward. Figure 4e exemplifies the reduction of the mass transfer profile as a result of enhancing Schmidt number Sc. Under the Schmidt number impact, the fluid's kinetic viscosity enlarges, and its mass transfer coefficient, $\phi(\eta)$, decreases. In figure 4f, it is detected that an enlargement of the Casson factor B, enhances the concentration curve. Physically, elevating the Casson fluid factor intensifies concentration curves by enhancing yield stress, escalating flow resistance, and thereby facilitating solute dispersion, resulting in enhanced concentration gradients within the system.

Table 1 demonstrates the experimental values and thermochemical features of the base fluid and the hybrid nanofluids. Table 2 confirms the legality of the present report to the published work. In Table 3, the absolute skin friction, Nusselt number, and Sherwood number are numerically computed for distinct, marked factors in the case of both hybrid and tri-hybrid nanofluid. The absolute shear stress for both hybrid and tri-hybrid nanofluid is enhanced for the term M, Fr and P, but dwindle for the Casson factor B. In the case of activation energy term E, the rate of thermal transport is enhanced. On the contrary, a reduction in the heat transportation rate is reported for escalating values of M, ϵ, Fr, B and P. Furthermore, an escalation in the rate of mass transport is noticed for enhancing ϵ, Sc and Cr. But the opposite pattern is noticed for enlarging E, M, Fr, B and P. Also, it has been asserted that ternary hybrid nanofluid has superior thermal and mass allocation percentage to hybrid nanofluid. It is also cleared from the table that the thermal transport rate for polymer-based trihybrid nanofluid is almost 3% superior in contrast to hybrid nanofluid.

As demonstrated in table 4, enhancing the volume proportion of MoS_2 nanoparticles whenever maintaining $\phi_1 = 0.02$ and ϕ_3 at zero, escalates the absolute shear rate, Nusselt number, and Sherwood number for the hybrid nanofluid. Also, it is reported that while keeping $\phi_1 = \phi_3 = 0.02$, boosting the

volume fraction of MoS_2, the rate of shear, thermal transmission, and mass transmission also enlarged. The core findings displayed that while the volume proportion of MoS_2 is kept constant at 0.02, the tri hybrid nanofluid illustrates an enhancement in the absolute shear rate up to 5.2%, and in the rate of thermal transport up to 3.05% in comparison to hybrid nanofluid.

4. CONCLUSION:

The primary goal of the study is to contemplate the heat and mass transmit aspect of polymer-based shear thinning ternary hybrid-nanofluid through the exponential stretching cylinder with an externally induced magnetic field. The activation energy, chemical reaction, variable thermal conductivity, and Darcy-Forchheimer impact are also investigated. Incorporating those terms reinforced the uniqueness of the flow model. By varying the distinct physical terms, flow, heat, and mass transport characteristics have been illustrated with the succor of graphs for both hybrid and ternary hybrid nanofluid. The rate of heat and mass transmission is calculated numerically and presented in the form of tables. This study also includes a strong comparison assessment. The following are the key attributes:

- The magnetic term, Casson factor, Darcy Forchhemier term, and porosity factor all have a negative influence on the velocity profiles.
- The positive deviations of $\epsilon, M, Fr, B,$ and P leads to an enhancement in the thermal profile.
- Incremented $E, B, M,$ and Fr escalates the concentration curve, but the reverse trend is reported for Cr and Sc.
- The chemical reaction, variable thermal conductivity, and Schmidt number positively affect the mass transport, since they accelerate the rapid motion of fluid particles, while the influence of activation energy, Casson term, and Darcy Forchhemier factor shrinks the mass transport rate.
- The thermal transmit rate is enhanced by the boosting activation energy. On the contrary, a dwindle is reported in the thermal transmission rate for escalating M, ϵ, Fr, B and P.
- The thermal transport rate for polymer-based trihybrid nanofluid is superior in contrast to hybrid nanofluid. $Ag - MoS_2 - Cu$/polymer tri-hybrid nanofluid appears to report an enhancement in the rate of thermal transport up to 3.05% in comparison to $Ag - MoS_2$/ Polymer hybrid nanofluid.
- $Ag - MoS_2 - Cu$/polymer tri-hybrid nanofluid illustrates an enhancement in the absolute shear rate up to 5.2% in contrast to $Ag - MoS_2$/polymer hybrid nanofluid.

NOMENCLATURE:

T	Temperature of the fluid (K)
T_w	Temperature at the wall (K)
T_∞	Ambient fluid temperature (K)
C	Concentration of hybrid nanofluid (Kg/m^3)
C_w	Concentration of hybrid nanofluid at wall (Kg/m^3)
C_∞	Ambient concentration of hybrid nanoparticle (Kg/m^3)
D	Mass diffusivity (m^2/s)
M	Magnetic term
E	Activation energy factor
Pr	Prandtl number
Sc	Schmidt number
Re	Reynolds number
N	Proportionality ratio parameter

Fr	Darcy-Forchheimer factor
P	Porosity Parameter
ϵ	Variable conductivity term
Cr	Chemical reaction parameter
γ	Temperature ratio parameter
B	Casson term
B_0	Dimensional magnetic field (NmA^{-1})
$\mu_{f,}\mu_{thnf}$	Dynamic viscosity of fluid and tri-hybrid nanofluid (mPa)
$\sigma_{f,}\sigma_{thnf}$	The electric conductivity of the fluid and tri-hybrid nanofluid($Ohm^{-1}m^{1}$)
$(C_p)_f, (C_p)_{thnf}$	Fluid and tri-hybrid nanofluid's specific heat capacity($Jkg^{-1}K^{-1}$)
k_f, k_{thnf}	Fluid and tri-hybrid nanofluid's thermal conductivity($Wm^{-1}K^{-1}$)
ρ_f, ρ_{thnf}	Fluid and tri-hybrid nanofluid's density(kgm^{-3})
ϕ_1	Volume proportion of Ag nanoparticle
ϕ_2	Volume proportion of MoS_2 nanoparticle
ϕ_3	Volume proportion of Cu nanoparticle
$thnf$	Ternary hybrid nanofluid
hnf	Hybrid nanofluid
nf	Nano fluid

Data availability statement: All data that support the findings of this study are included within the article.

Conflict of interest: Authors have no Conflict of interest.

Financial interests: Authors have no financial interests.

Authors' contributions: All the authors have contributed equally in the preparation of the manuscript.

REFERENCES:

1. Kakaç, S. and Pramuanjaroenkij, A. "Review of convective heat transfer enhancement with nanofluids", *Int. J. Heat Mass Transf.*, **52**(13-14), pp.3187-3196 (2009).https://doi.org/10.1016/j.ijheatmasstransfer.2009.02.006
2. Kumar, P. and Sarviya, R.M. "Recent developments in preparation of nanofluid for heat transfer enhancement in heat exchangers: A review", *Mater. Today*, **44**, pp.2356-2361 (2021). https://doi.org/10.1016/j.matpr.2020.12.434
3. Shrestha, K., Wong, E., Salati, H., et al. "Liquid volume and squeeze force effects on nasal irrigation using Volume of Fluid modelling", *Exp. Comput. Multiph. Flow.*, pp.1-20 (2022). https://doi.org/10.1007/s42757-021-0123-5
4. Arulmozhi, S., Sukkiramathi, K., Santra, S.S., et al. "Heat and mass transfer analysis of radiative and chemical reactive effects on MHD nanofluid over an infinite moving vertical plate", *Results Eng.*, **14**, p.100394 (2022). https://doi.org/10.1016/j.rineng.2022.100394
5. Reddy, Y.D. and Mangamma, I. "Significance of radiation and chemical reaction on MHD heat transfer nanofluid flow over a nonlinearly porous stretching sheet with nonuniform heat source", *Numer. Heat Transf. A*, pp.1-27 (2023). https://doi.org/10.1080/10407782.2023.2230356
6. Ahmad, S., Ali, K., Rizwan, M., et al. "Heat and mass transfer attributes of copper–aluminum oxide hybrid nanoparticles flow through a porous medium", *Case Stud. Therm. Eng.*, **25**, p.100932 (2021). https://doi.org/10.1016/j.csite.2021.100932
7. Kavya, S., Nagendramma, V., Ahammad, N.A., et al. "Magnetic-hybrid nanoparticles with stretching/shrinking cylinder in a suspension of MoS4 and copper nanoparticles", *Int. Commun. Heat Mass Transf.*, **136**, p.106150 (2022). https://doi.org/10.1016/j.icheatmasstransfer.2022.106150
8. Vijatha, M. and Reddy, P.B.A. "Entropy optimization of magnetohydrodynamic hybrid nanofluid flow with Cattaneo-Christov heat flux model", *Sci. Iran.*, **29**(6), pp.3603-3618 (2022). https://doi.org/10.24200/sci.2022.60107.6599
9. Paul, A., Das, T.K. and Nath, J.M. "Numerical investigation on the thermal transportation of MHD Cu/Al 2 O 3-H 2 O Casson-hybrid-nanofluid flow across an exponentially stretching cylinder incorporating heat source", *Phys. Scr.*, **97**(8), p.085701 (2022). https://doi.org/10.1088/1402-4896/ac7981
10. Paul, A., Mani Nath, J. and Kanti Das, T. "An investigation of the MHD Cu-Al 2 O 3/H 2 O hybrid-nanofluid in a porous medium across a vertically stretching cylinder incorporating thermal stratification impact", *J. Therm. Eng.*, **9**(3), pp. 799−810 (2023). https://doi.org/10.18186/thermal.1300847
11. Paul, A., Nath, J.M. and Das, T.K. "Thermally stratified Cu–Al2O3/water hybrid nanofluid flow with the impact of an inclined magnetic field, viscous dissipation and heat source/sink across a vertically stretching cylinder", *ZAMM Z. fur Angew. Math. Mech.*, **104**, p. e202300084 (2024). https://doi.org/10.1002/zamm.202300084
12. Chu, Y.M., Bashir, S., Ramzan, M., et al. "Model-based comparative study of magnetohydrodynamics unsteady hybrid nanofluid flow between two infinite parallel plates with particle shape effects", *Math. Methods Appl. Sci.*, **46**(10), pp.11568-11582 (2023). https://doi.org/10.1002/mma.8234
13. Shamshuddin, M.D., Agbaje, T.M., Asogwa, K.K., et al. "Computational investigation for silica-molybdenum disulfide/water-based hybrid nanofluid over an exponential stretching sheet

with spectral quasi-linearization method", *Numer. Heat Transf. B: Fundam.*, pp.1-25 (2023). https://doi.org/10.1080/10407790.2023.2289503

14. Shamshuddin, M.D., Salawu, S.O., Ramesh, K., et al. "Bioconvective treatment for the reactive Casson hybrid nanofluid flow past an exponentially stretching sheet with Ohmic heating and mixed convection", *J. Therm. Anal. Calorim.*, **148**(21), pp.12083-12095 (2023). https://doi.org/10.1007/s10973-023-12465-x
15. Lone, S.A., Shamshuddin, M.D., Shahab, S., et al. "Computational analysis of MHD driven bioconvective flow of hybrid Casson nanofluid past a permeable exponential stretching sheet with thermophoresis and Brownian motion effects", *J. Magn. Magn. Mater.*, **580**, p.170959 (2023). https://doi.org/10.1016/j.jmmm.2023.170959
16. Tamanna, M.N., Ferdows, M., Lorenzini, G., et al. "Numerical Investigation of Heat Transfer Enhancement on Tangent Hyperbolic Fluid over a Stretching Sheet with an Inclined Magnetic Field Filled with Hybrid Nanofluids", *J. Eng. Thermophys.*, **33**(1), pp.55-72 (2024). https://doi.org/10.1134/S1810232824010065
17. Yasmin, H., Lone, S.A., Mahnashi, A.M., et al. "Optimized framework numerical solution for swirling hybrid nanofluid flow with silver/gold nanoparticles on a stretching cylinder with heat source/sink and reactive agents", *Open Phys.*, **22**(1), p.20230202 (2024). https://doi.org/10.1515/phys-2023-0202
18. Shamshuddin, M.D., Saeed, A., Mishra, S.R., et al. "Homotopic simulation of MHD bioconvective flow of water-based hybrid nanofluid over a thermal convective exponential stretching surface", *Int. J. Numer. Methods Heat Fluid Flow.*, **34**(1), pp.31-53 (2024). https://doi.org/10.1108/HFF-03-2023-0128
19. Manjunatha, S., Puneeth, V., Gireesha, B.J., et al. "Theoretical study of convective heat transfer in ternary nanofluid flowing past a stretching sheet", *J. Appl. Comput. Mech.*, **8**(4), pp.1279-1286 (2022). https://doi.org/10.22055/jacm.2021.37698.3067
20. Alharbi, K.A.M., Ahmed, A.E.S., Ould Sidi, M., et al. "Computational valuation of Darcy ternary-hybrid nanofluid flow across an extending cylinder with induction effects", *Micromachines*, **13**(4), p.588 (2022). https://doi.org/10.3390/mi13040588
21. Nagaraja, K.V., Khan, U., Madhukesh, J.K., et al. "Heat and mass transfer analysis of assisting and opposing radiative flow conveying ternary hybrid nanofluid over an exponentially stretching surface", *Sci. Rep.*, **13**(1), p.14795 (2023). https://doi.org/10.1038/s41598-023-41916-6
22. Mumtaz, M., Islam, S., Ullah, H., et al. "Chemically reactive MHD convective flow and heat transfer performance of ternary hybrid nanofluid past a curved stretching sheet", *J. Mol. Liq.*, **390**, p.123179 (2023). https://doi.org/10.1016/j.molliq.2023.123179
23. Jayaprakash, M.C., Alsulami, M.D., Shanker, B., et al. "Investigation of Arrhenius activation energy and convective heat transfer efficiency in radiative hybrid nanofluid flow", *Waves Random Complex Media.*, pp.1-13 (2022). https://doi.org/10.1080/17455030.2021.2022811
24. Rekha, M.B., Sarris, I.E., Madhukesh, J.K., et al. "Activation energy impact on flow of AA7072-AA7075/Water-Based hybrid nanofluid through a cone, wedge and plate", *Micromachines*, **13**(2), p.302 (2022). https://doi.org/10.3390/mi13020302
25. Mishra, N.K., Sharma, B.K., Sharma, P., et al. "Entropy generation optimization of cilia regulated MHD ternary hybrid Jeffery nanofluid with Arrhenius activation energy and induced magnetic field", *Sci. Rep.*, **13**(1), p.14483 (2023). https://doi.org/10.1038/s41598-023-41299-8
26. Puneeth, V., Manjunatha, S., Anwar, M.S., et al. "Stratified bioconvective jet flow of williamson nanofluid in porous medium in the presence of Arrhenius activation energy", *J.*

Comput. Biophys. Chem., **22**(03), pp.309-319 (2023). https://doi.org/10.1142/S2737416523400069

27. Zubair, T., Usman, M., Hamid, M., et al. "Computational analysis of radiative Williamson hybrid nanofluid comprising variable thermal conductivity", *Jpn. J. Appl. Phys.*, **60**(8), p.087004 (2021). https://doi.org/10.35848/1347-4065/ac1388
28. Eid, M.R. and Nafe, M.A. "Thermal conductivity variation and heat generation effects on magneto-hybrid nanofluid flow in a porous medium with slip condition", *Waves Random Complex Media.*, **32**(3), pp.1103-1127 (2022). https://doi.org/10.1080/17455030.2020.1810365
29. Manigandan, A. and Satya Narayana, P.V. "Influence of variable thermal conductivity and mixed convection on hybrid nanofluid (SWCNT+ MWCNT/H2O) flow over an exponentially elongated sheet with slip conditions", *Ind. J. Phys.*, **98**, pp.1401-1414 (2024). https://doi.org/10.1007/s12648-023-02912-8
30. Jan, S.U., Khan, U., Islam, S., et al. "Impact of variable thermal conductivity on flow of trihybrid nanofluid over a stretching surface", *Nanotechnol.*, **34**(46), p.465301 (2023). https://doi.org/10.1088/1361-6528/acedb4
31. Gautam, A.K., Verma, A.K., Bhattacharyya, K., et al. "Impacts of activation energy and binary chemical reaction on MHD flow of Williamson nanofluid in Darcy–Forchheimer porous medium: A case of expanding sheet of variable thickness", *Waves Random Complex Media.*, pp.1-22 (2021). https://doi.org/10.1080/17455030.2021.1979274
32. ur Rahman, M., Haq, F., Khan, M.I., et al. "Irreversibility analysis in viscous nanomaterial flow with Darcy–Forchheimer and activation energy", *Int. J. Appl. Comput. Math.*, **8**(6), p.270 (2022). https://doi.org/10.1007/s40819-022-01460-9
33. Haq, I., Yassen, M.F., Ghoneim, M.E., et al. "Computational study of MHD Darcy–Forchheimer hybrid nanofluid flow under the influence of chemical reaction and activation energy over a stretching surface", *Symmetry*, **14**(9), p.1759 (2022). https://doi.org/10.3390/sym14091759
34. Alqahtani, A.M., Bilal, M., Usman, M., et al. "Heat and mass transfer through MHD Darcy Forchheimer Casson hybrid nanofluid flow across an exponential stretching sheet", *ZAMM Z. fur Angew. Math. Mech.*, **103**, p. e202200213 (2023). https://doi.org/10.1002/zamm.202200213
35. Ramasekhar, G. and Bala Anki Reddy, P. "Entropy generation on Darcy-Forchheimer flow of copper-aluminium oxide/water hybrid nanofluid over a rotating disk: Semi-analytical and numerical approaches", *Sci. iran.*, **30**(6), pp.2245-2259 (2023). https://doi.org/10.24200/sci.2023.60134.6617
36. Zeeshan, A., Khan, M.I., Ellahi, R., et al. "Computational intelligence approach for optimising MHD Casson ternary hybrid nanofluid over the shrinking sheet with the effects of radiation", *Appl. Sci.*, **13**(17), p.9510 (2023). https://doi.org/10.3390/app13179510
37. Turabi, Y.U.U.B., Munir, S. and Amin, A. "Numerical analysis of convective transport mechanisms in two-layer ternary (TiO 2− SiO 2− Al 2 O 3) Casson hybrid nanofluid flow in a vertical channel with heat generation effects", *Numer. Heat Transf. A*, pp.1-15 (2023). https://doi.org/10.1080/10407782.2023.2281542
38. Ali, G., Kumam, P., Sitthithakerngkiet, K., et al. "Heat transfer analysis of unsteady MHD slip flow of ternary hybrid Casson fluid through nonlinear stretching disk embedded in a porous medium", *Ain Shams Eng. J.*, **15**(2), p.102419 (2024). https://doi.org/10.1016/j.asej.2023.102419

39. Paul, A. and Das, T.K. “Darcy–Forchheimer MHD radiative flow through a porous space incorporating viscous dissipation, heat source, and chemical reaction effect across an exponentially stretched surface”, *Heat Transf.*, **52**(1), pp.807-825 (2023). https://doi.org/10.1002/htj.22717
40. Upreti, H., Pandey, A.K., Joshi, N., et al. “Thermodynamics and heat transfer analysis of magnetized Casson hybrid nanofluid flow via a Riga plate with thermal radiation”, *J. Comput. Biophys. Chem.*, **22**(03), pp.321-334 (2023). https://doi.org/10.1142/S2737416523400070
41. Abbas, M., Khan, N., Hashmi, M.S., et al. “Importance of thermophoretic particles deposition in ternary hybrid nanofluid with local thermal non-equilibrium conditions: Hamilton–Crosser and Yamada–Ota models”, *Case Stud. Therm. Eng.*, **56**, p.104229 (2024). https://doi.org/10.1016/j.csite.2024.104229
42. Mahmood, Z., Iqbal, Z., Alyami, M.A., et al. “Influence of suction and heat source on MHD stagnation point flow of ternary hybrid nanofluid over convectively heated stretching/shrinking cylinder”, *Adv. Mech. Eng.*, **14**(9), p.16878132221126278 (2022). https://doi.org/10.1177/16878132221126278
43. Mahmood, Z. and Khan, U. “Unsteady three-dimensional nodal stagnation point flow of polymer-based ternary-hybrid nanofluid past a stretching surface with suction and heat source”, *Sci. Prog.*, **106**(1), p.00368504231152741 (2023). https://doi.org/10.1177/00368504231152741
44. Basit, M.A., Farooq, U., Imran, M., et al. “Comprehensive investigations of (Au-Ag/Blood and Cu-Fe3O4/Blood) hybrid nanofluid over two rotating disks: Numerical and computational approach”, *Alex. Eng. J.*, **72**, pp.19-36 (2023). https://doi.org/10.1016/j.aej.2023.03.077
45. Ishak, A., Nazar, R. and Pop, I. “Uniform suction/blowing effect on flow and heat transfer due to a stretching cylinder”, *Appl. Math. Model.*, **32**(10), pp.2059-2066 (2008). https://doi.org/10.1016/j.apm.2007.06.036

Biographies of the Authors:

Jintu Mani Nath: Mr. Jintu Mani Nath is an Assistant professor in the Department of Mathematics at Mangaldai College, Assam, India. Also, he is a senior research scholar pursuing PhD program in the Department of Mathematics at Cotton University, Guwahati, India. His current research interests include computational fluid dynamics and hybrid nanofluid flows. Mr. Nath has published 12 research articles in reputed international journals.

Prof. Ali J. Chamkha: Ali J. Chamkha is a Distinguished Professor of Mechanical Engineering and Dean of Engineering at Kuwait College of Science and Technology. He earned his Ph.D. in Mechanical Engineering from Tennessee Technological University, USA, in 1989. His research interests include multiphase fluid-particle dynamics, nanofluids dynamics, fluid flow in porous media, heat and mass transfer, magnetohydrodynamics, and fluid-particle separation. He is currently the Editor-in-Chief for the Journal of Nanofluids and has served as an Editor, Associate Editor, or a member of the editorial board for many reputed journals. He has authored and co-authored over 1250 publications in archival international journals and conferences. His current h-index is 141, and his total citations are more than 61,000.

Dr. Ashish Paul: Dr. Ashish Paul is working as an Associate Professor in the mathematics department at Cotton University, India. Previously, he served as an Assistant Professor at Bodoland University and Assam Don Bosco University in India. He received PhD in Mathematics from Gauhati University, India, in 2012. His research interests included Fluid Mechanics, heat and mass transfer, and hybrid nanofluid flow. He has published over 55 research articles in reputable international journals and conference proceedings.

Tusar Kanti Das: Mr. Tusar Kanti Das is an Assistant professor in the Department of Mathematics at Dudhnoi College, Assam, India. Also, he is a senior research scholar pursuing PhD in the Department of Mathematics at Cotton University, India. His Current Research interests are Magnetohydrodynamics, and hybrid nanofluids. Mr. Das has published 12 research articles in reputed international journals. His current Scopus h-index is 5.

Figures

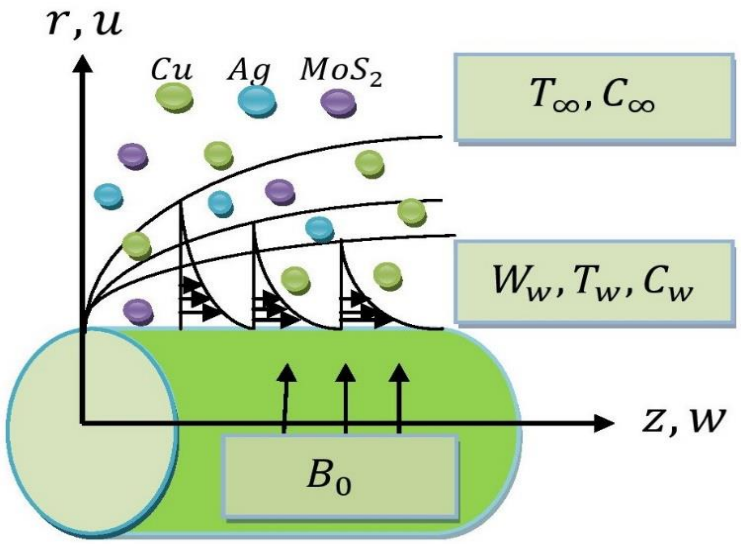

Figure 1. Pictorial demonstration of the flow model

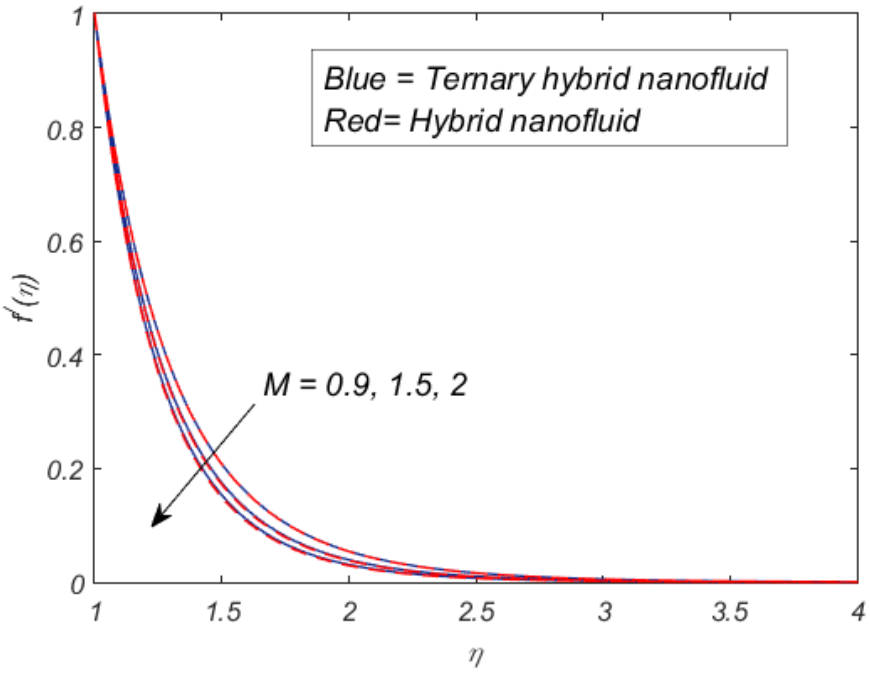

Figure 2a. Influence of M on velocity profile

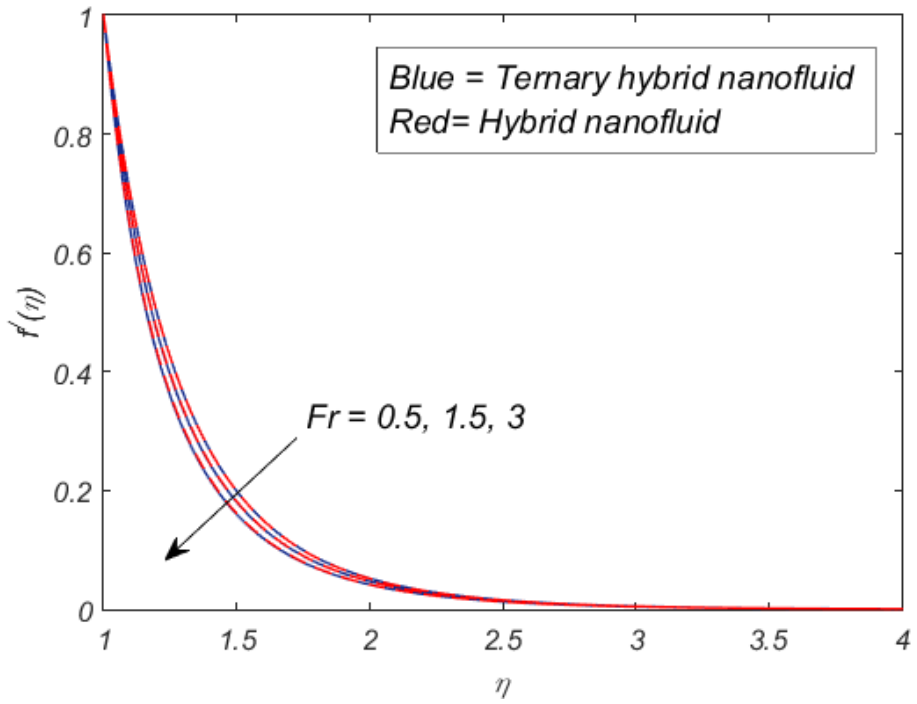

Figure 2b. Influence of Fr on velocity curve

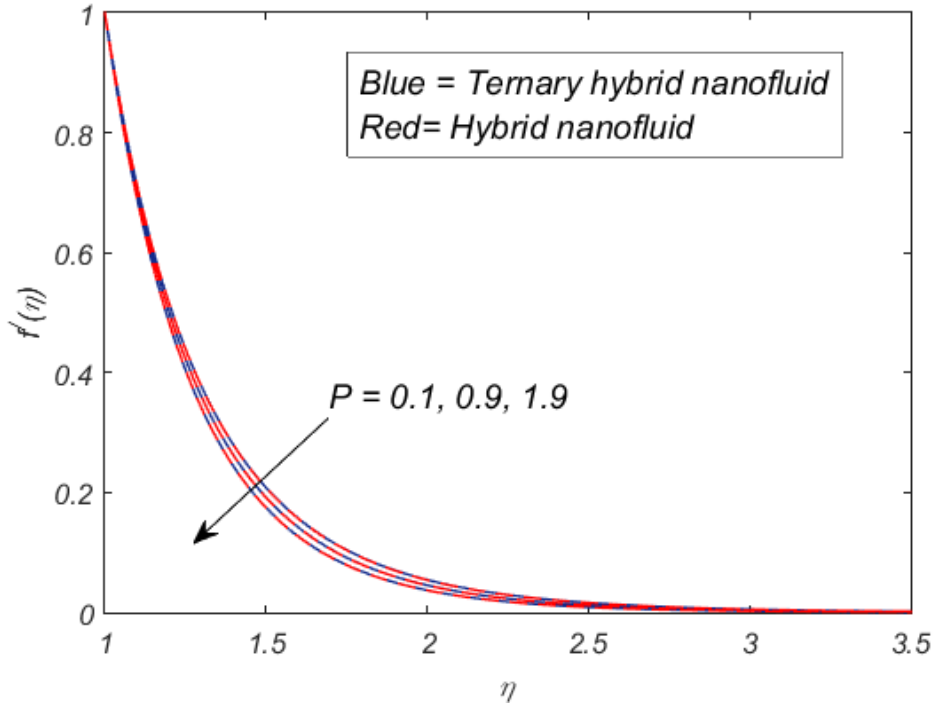

Figure 2c. Influence of P on velocity curve

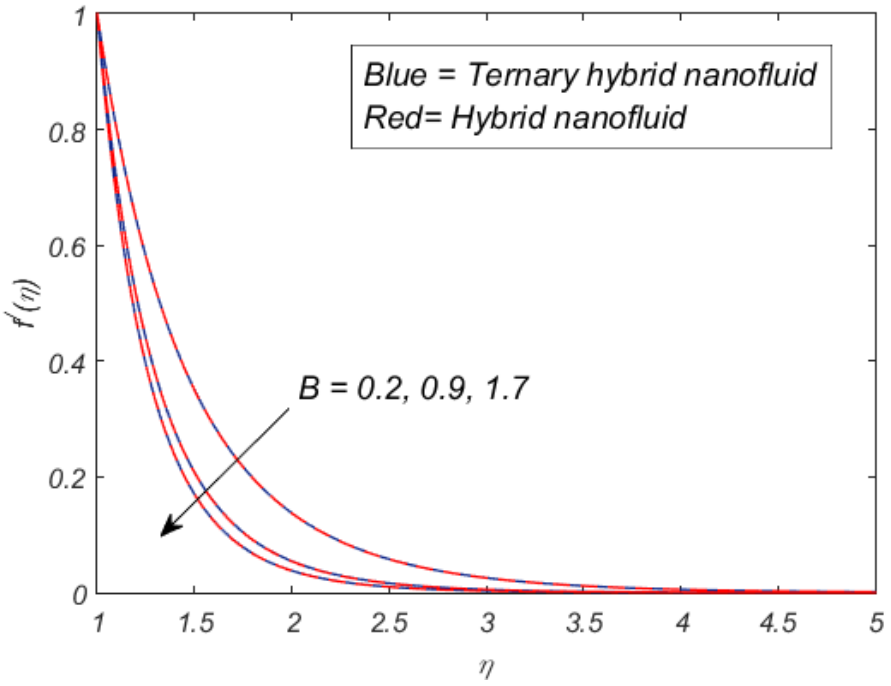

Figure 2d. Influence of B on velocity curve

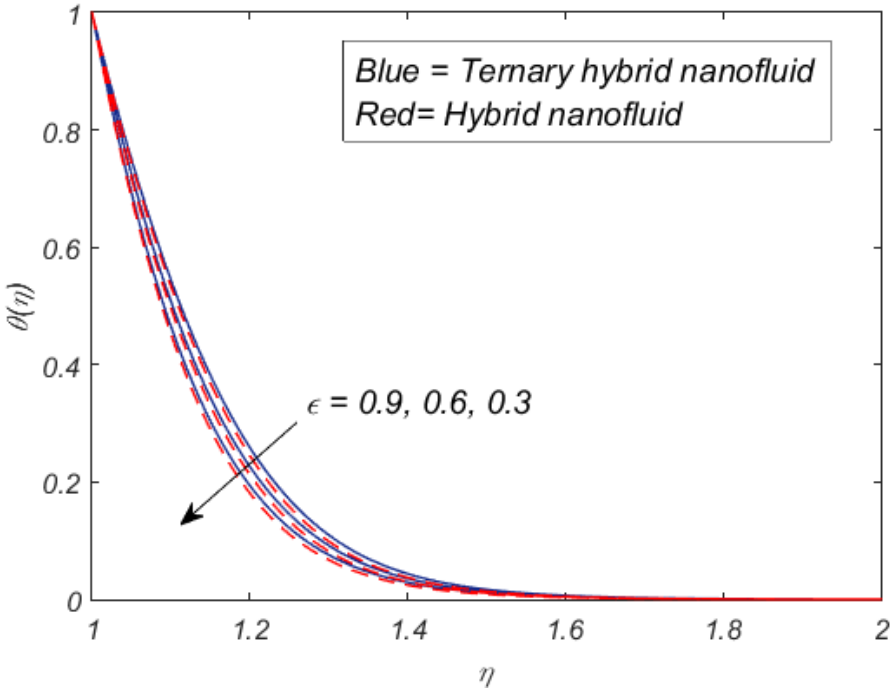

Figure 3a. Influence of ϵ on thermal curve

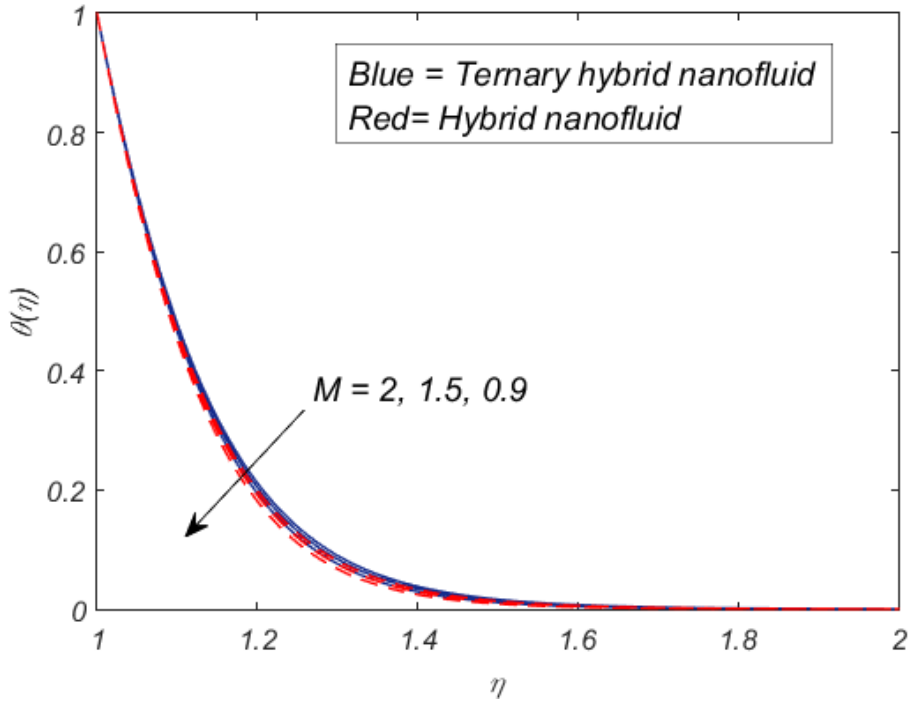

Figure 3b. Influence of M on thermal curve

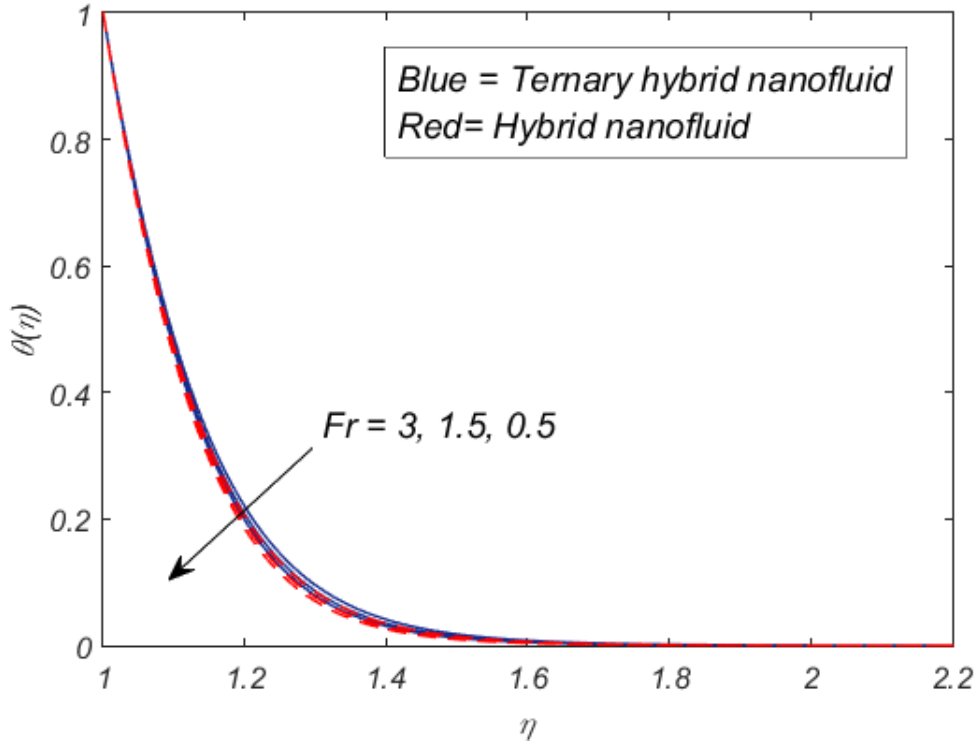

Figure 3c. Influence of Fr on thermal curve

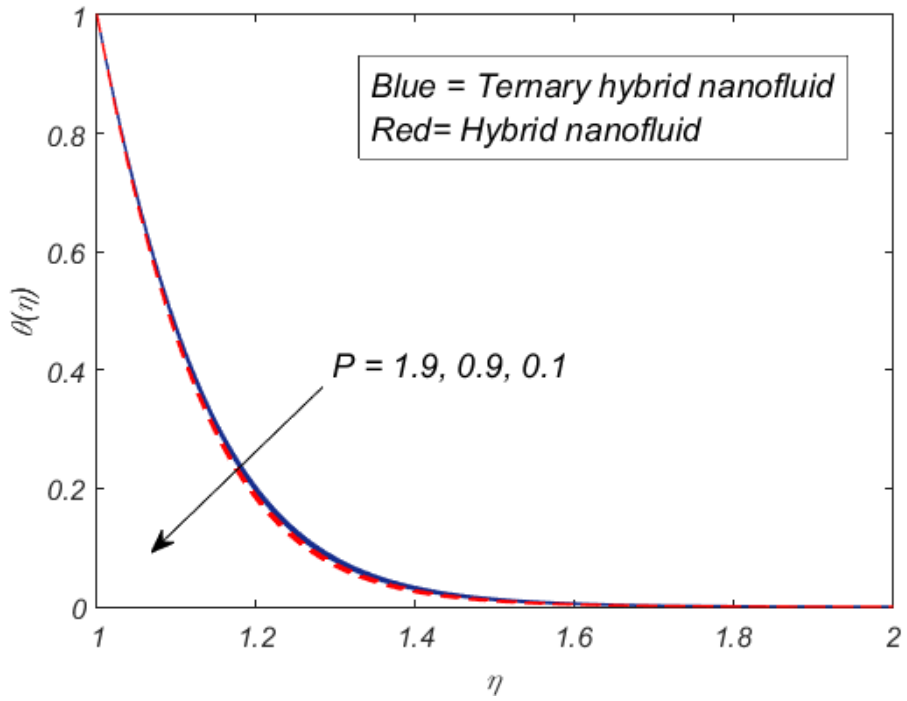

Figure 3d. Influence of P on thermal curve

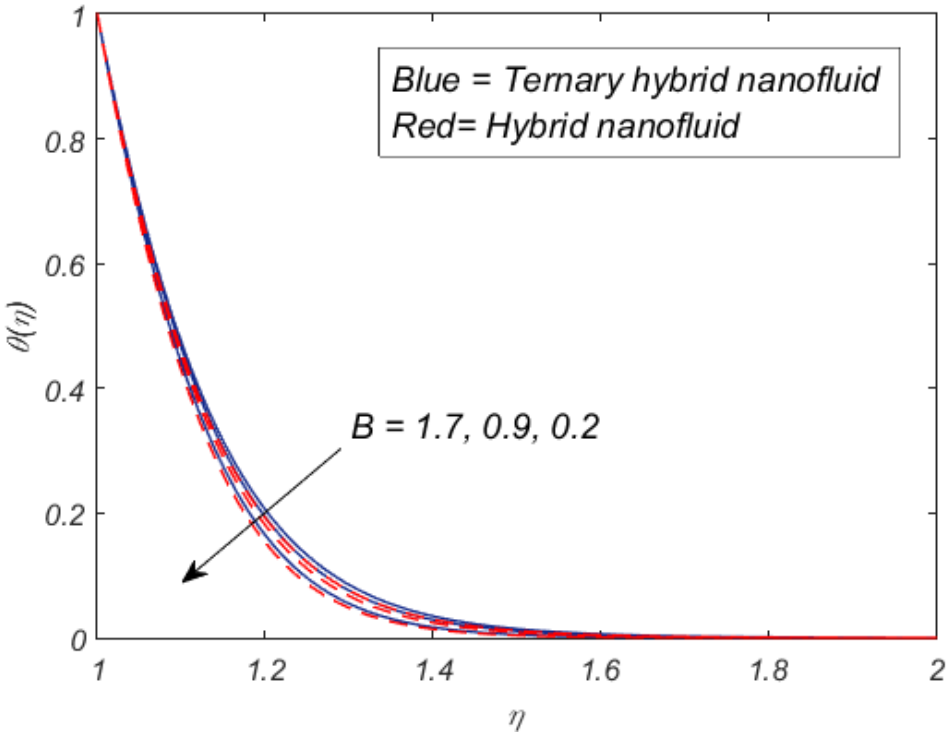

Figure 3e. Influence of B on thermal curve

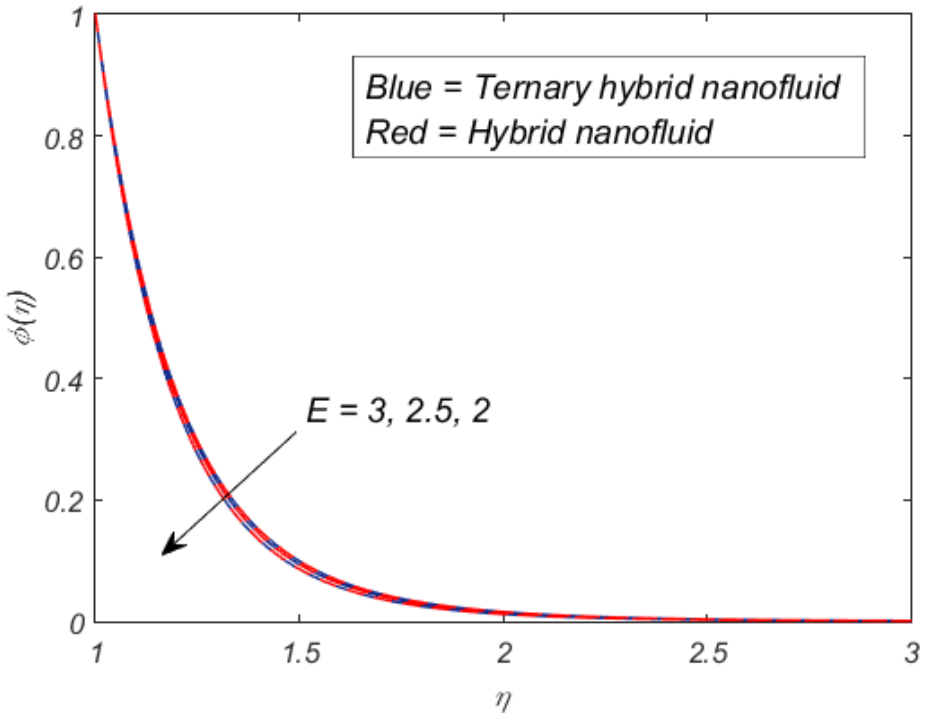

Figure 4a. Influence of E on concentration curve

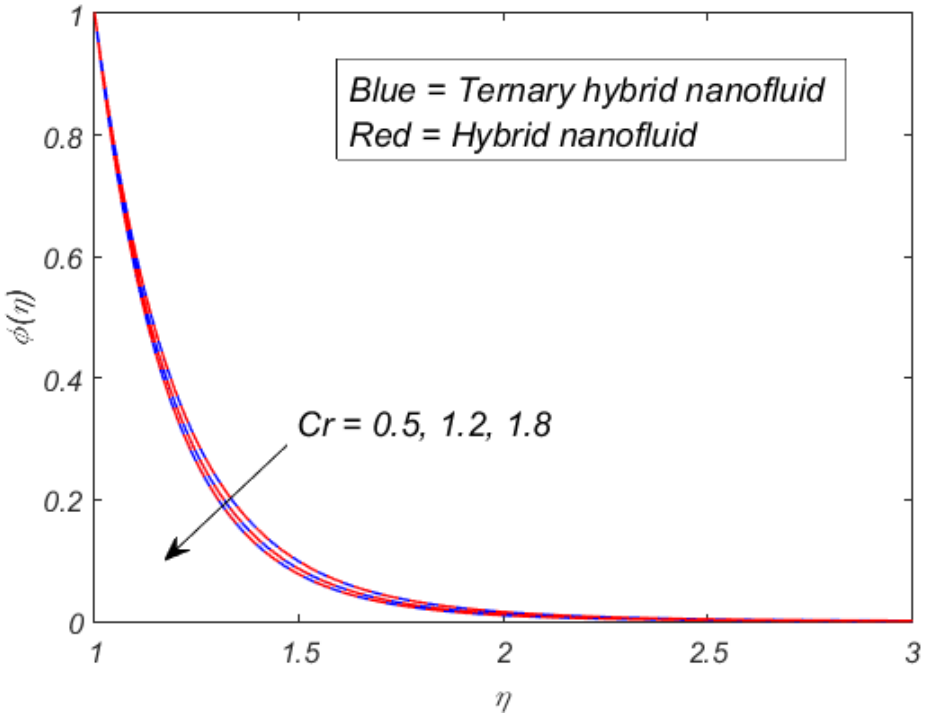

Figure 4b. Influence of Cr on concentration curve

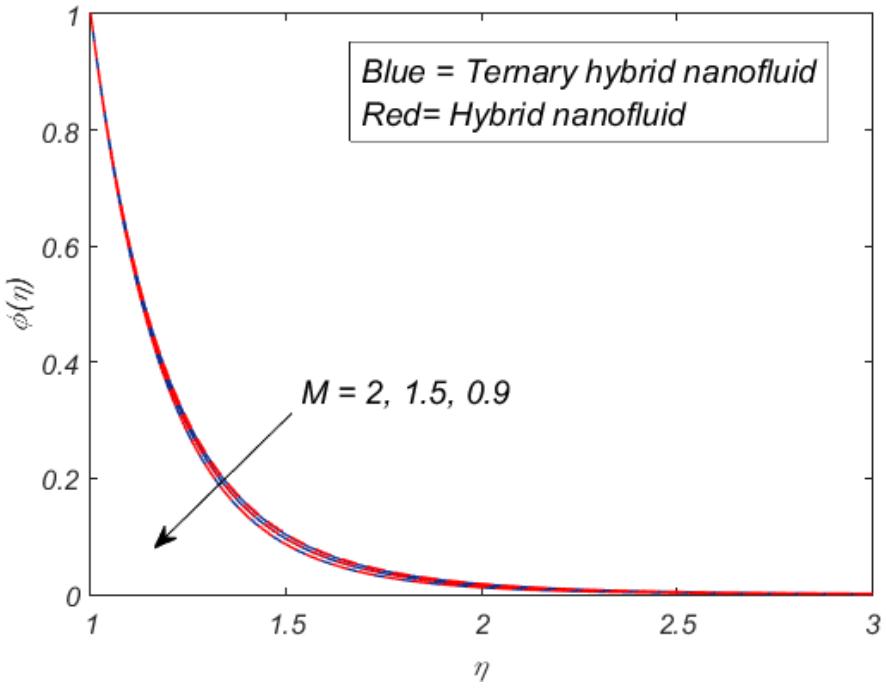

Figure 4c. Influence of M on concentration curve

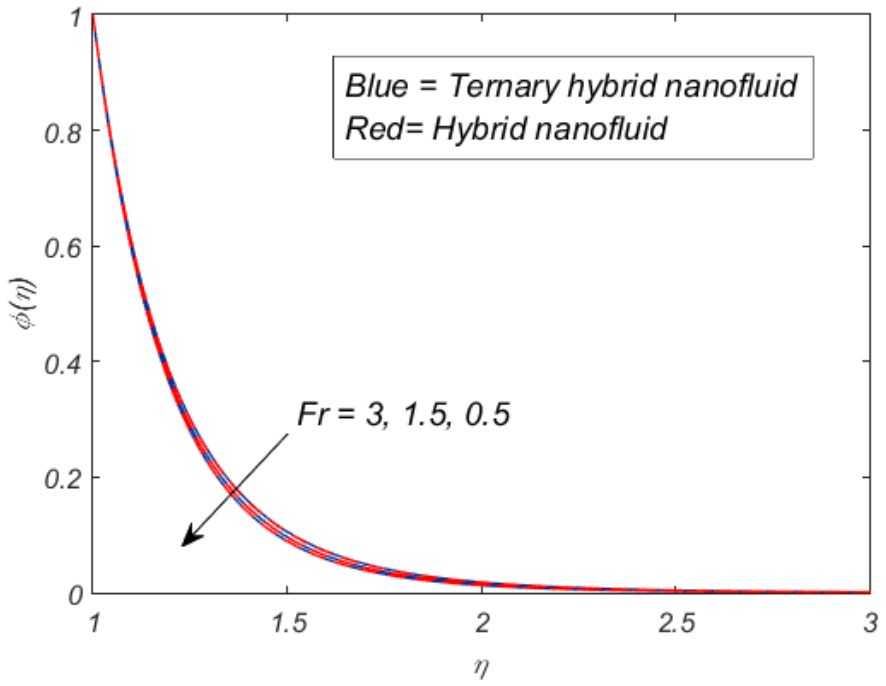

Figure 4d. Influence of Fr on concentration curve

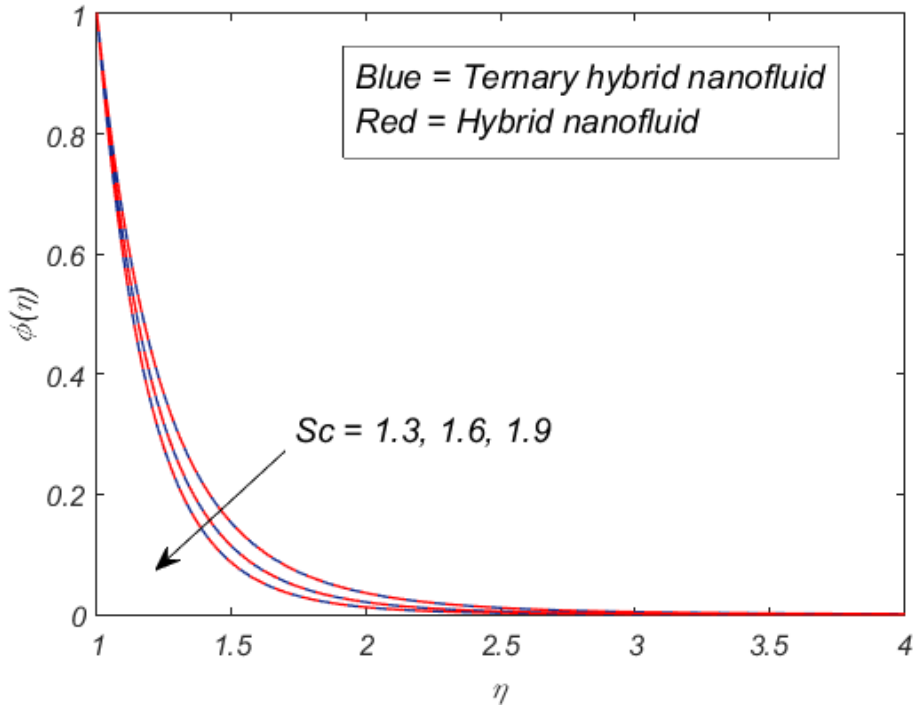

Figure 4e. Influence of Sc on concentration curve

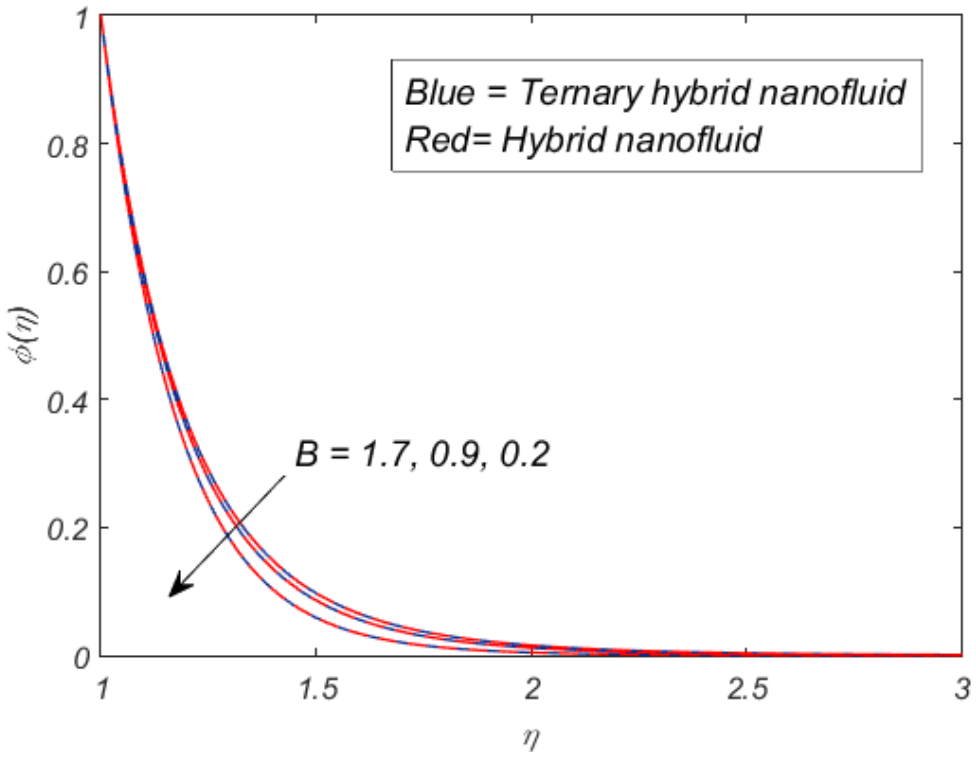

Figure 4f. Influence of B on concentration curve

TABLES

Table 1. Thermo-physical attributes of the nanoparticles and base fluid [Ref. [10], [42], [43], [44]]

Properties	Ag	MoS_2	Cu	Base fluid (Polymer)
$\rho\ (kg/m^3)$	10490	5060	8933	1060
$c_p\ (J/kgK)$	235	397.21	385	3770
$k(W/\ mK)$	429	904.4	400	0.429
$\sigma\ (S/m)$	6.30×10^7	2.09×10^4	59.6 x 10^6	4.3×10^{-5}

Table 2. Comparable findings with Ishak et al. [45]

Re	Ishak et al. [33]	Present study
0.5	-0.8827	-0.8824
1	-1.1781	-1.1778
2	-1.5941	-1.5939
5	-2.4175	-2.4174
10	-3.3445	-3.3445

Table 3. Computed findings for distinct physical components while $\phi_1 = \phi_2 = \phi_3 = 0.02$

Term	Value	Hybrid Nanofluid ($\phi_3 = 0$)			Ternary Hybrid Nanofluid		
		Skin friction	Nusselt Number	Sherwood number	Skin friction	Nusselt Number	Sherwood Number
E	2	-8.1080	24.2910	4.3653	-8.5310	25.0370	4.3689
	2.5	-8.1080	28.3395	4.1835	-8.5310	29.2099	4.1862
	3	-8.1080	32.3880	4.0630	-8.5310	33.3827	4.0650
M	0.9	-8.1080	24.2910	4.3653	-8.5310	25.0370	4.3689
	1.5	-9.0704	23.9608	4.2818	-9.4696	24.7090	4.2912
	2	-9.7954	23.7100	4.2201	-10.1811	24.4583	4.2339
ϵ	0.3	-8.1080	24.2910	4.3653	-8.5310	25.0370	4.3689
	0.6	-8.1080	21.1367	4.3760	-8.5310	21.8473	4.3795
	0.9	-8.1080	18.8544	4.3856	-8.5310	19.5263	4.3889
Sc	1.3	-8.1080	24.2910	4.3653	-8.5310	25.0370	4.3689
	1.6	-8.1080	24.2910	4.9117	-8.5310	25.0370	4.9156
	1.9	-8.1080	24.2910	5.4101	-8.5310	25.0370	5.4142
Cr	0.5	-8.1080	24.2910	5.0658	-8.5310	25.0370	5.0678
	1.2	-8.1080	24.2910	5.0658	-8.5310	25.0370	5.4142
	1.8	-8.1080	24.2910	5.0658	-8.5310	25.0370	5.6950
Fr	0.5	-8.5864	24.1587	5.3789	-9.0627	24.8886	5.3814
	1.5	-9.6817	23.8586	5.3092	-10.2751	24.5532	5.3084
	3	-11.1260	23.4687	5.2211	-11.8660	24.1204	5.2168
P	0.1	-8.1080	24.2910	5.4101	-8.5310	25.0370	5.4142
	0.9	-8.4426	24.1695	5.3772	-8.8834	24.9062	5.3813
	1.9	-8.8344	24.0271	5.3393	-9.2957	24.7532	5.3434
B	0.2	-15.0078	25.2316	5.6628	-15.7896	26.0436	5.6661
	0.9	-8.1080	24.2910	5.4101	-8.5310	25.0370	5.4142
	1.7	-6.9222	23.9209	5.3150	-7.2835	24.6407	5.3194

Table 4. Contrast of the Shear rate, heat transport, and mass transmission for hybrid and tri-hybrid nanofluid

Hybrid nanofluid ($Ag - MoS_2/Polymer$)						Ternary hybrid nanofluid ($Ag - MoS_2 - Cu/Polymer$)					
ϕ_1	ϕ_2	ϕ_3	Skin Friction	Nusselt Number	Sherwood Number	ϕ_1	ϕ_2	ϕ_3	Skin Friction	Nusselt Number	Sherwood Number
0.02	0.02	0	-8.1080	24.2910	5.4101	0.02	0.02	0.02	-8.5310	25.0370	5.4142
	0.03		-8.3093	24.6178	5.4131		0.03		-8.7365	25.3714	5.4177
	0.04		-8.5152	24.9433	5.4163		0.04		-8.9468	25.7045	5.4214
	0.05		-8.7259	25.2677	5.4198		0.05		-9.1621	26.0367	5.4253